THERMODYNAMIC ASSESSMENT OF THE Al–Mo–V TERNARY SYSTEM

B. Hu [a,*], B. Yao [a], J. Wang [b,*], J.-R. Zhao [c], F.-F. Min [a], Y. Du [b]

[a] Anhui University of Science and Technology, School of Materials Science and Engineering, Huainan, China
[b] Central South University, State Key Laboratory of Powder Metallurgy, Changsha, China
[c] Shandong Academy of Sciences, Advanced Materials Institute, Shandong Key Laboratory for High Strength Lightweight Metallic Materials (HLM), Shandong Engineering Research Center for Lightweight Automobiles Magnesium Alloy, Jinan, China

Abstract

Thermodynamic assessment of the Al–Mo–V ternary system was performed by means of the CALPHAD (CALculation of PHAse Diagram) approach based on the thermodynamic descriptions of three constitutive binary systems (Al–Mo, Al–V and Mo–V) as well as the experimental phase equilibria data available in the literature. The solution phases, i.e. liquid, bcc (Mo, V) and fcc (Al), were described using the substitutional solution models with the Redlich-Kister equation. The binary phases in the Al–Mo and Al–V systems with the solubilities of the third element were modeled using the sublattice models. An optimal set of thermodynamic parameters for the Al–Mo–V system was obtained. Six isothermal sections at 1200, 1000, 750, 715, 675 and 630 °C and liquidus projection with isotherm were calculated. The reaction scheme for the entire Al–Mo–V system was also constructed. Comparisons between the calculated and measured phase diagrams indicated that almost all the reliable experimental information was satisfactorily accounted for by the present modeling.

Keywords: Al–Mo–V system; CALPHAD approach; Isothermal section; Liquidus projection

1. Introduction

Al–Mo–V ternary system is of great interest because it is an important sub-system in Al-based and Ti-based alloys. In Al-based alloys, Mo and V as two of the common additional elements improve the performance of the Al-based alloys [1-4]. In Ti-based alloys, additions of transition metal elements such as Mo and V to titanium can stabilize the high temperature β phase to room temperature following rapid cooling. Mo and V are the most frequently used β isomorphous elements in Ti-based alloys [5]. In addition, Mo can improve the quenchability of the β phase in TiAl-based alloys [6, 7] and V can improve the room-temperature ductility of TiAl and Ti_3Al alloys [8]. The design of compositions of Al or Ti based novel alloys requires information about the phase equilibria of the Al–Mo–V ternary system. Therefore, a thorough thermodynamic assessment of the Al–Mo–V system is necessary for providing a set of reliable thermodynamic parameters for thermodynamic extrapolations to related higher order systems.

Thermodynamic description for the Al–Mo–V system is part of our efforts [9-17] to establish thermodynamic databases of multi-component Al and/or Ti based alloys. To the best of our knowledge, thermodynamic description for the Al–Mo–V system is not available in the literature nor in commercial database [18]. The purposes of the present work are to critically evaluate the measured phase diagram data available in the literature and to obtain a set of self-consistent thermodynamic parameters for the Al–Mo–V systems by means of the CALPHAD approach [19, 20].

2. Evaluation of experimental data

To facilitate reading, the symbols used to denote the solid phases in the Al–Mo–V system are listed in Table 1. The Gibbs energy functions for the pure elements Al, Mo and V are taken from the SGTE (Scientific Group Thermodata Europe) database compiled by Dinsdale [21]. The thermodynamic parameters for Al–Mo, Al–V, and Mo–V systems are taken from Peng et al. [22], Gong et al. [23] and Zheng et al. [24], respectively. In particular, Peng et al. [22] refined the thermodynamic parameters of the Al–Mo system based on the work of Cupid et al.[7]. A

set of thermodynamic parameters of the Mo–V binary system is taken from Zheng et al. [24] rather than the newer one from Bratberg and Frisk [25]. On the one hand, the thermodynamic parameters of the Mo–V system from Zheng et al. [24] are consistent with the multi-component alloys database developed by our research group [16]. On the other hand, the calculated results from Bratberg and Frisk show a miscibility gap in the bcc phase below 1160 K without experimental evidence. For the Al–V system, the thermodynamic parameters are adopted from our own group [23] rather than Lindahl et al.[26] also in order to be consistent with the database of our group. The calculated three constitutive binary systems are presented in Fig. 1 (a) to (c).
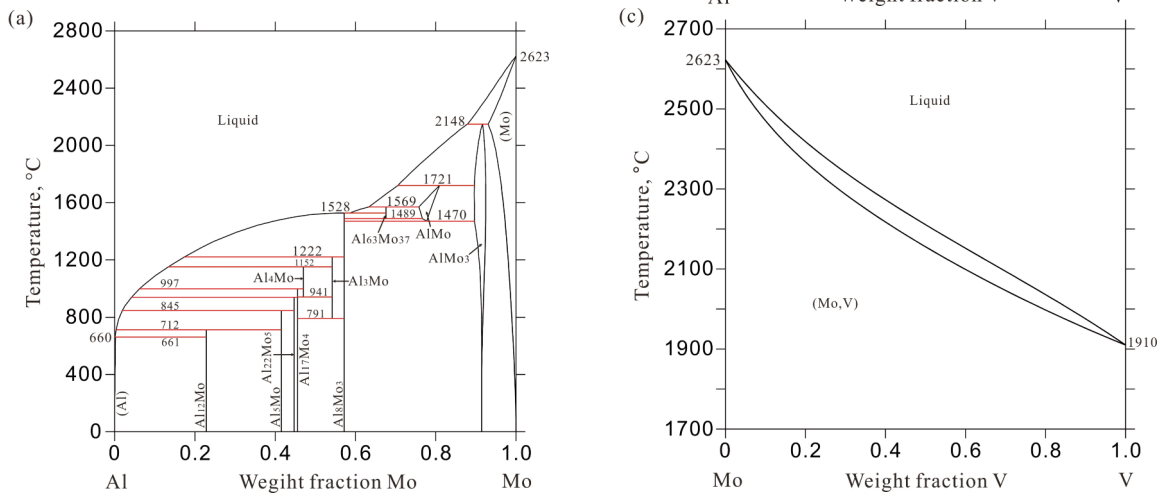

Figure 1. Calculated binary phase diagrams: (a) Al–Mo system [22], (b) Al–V system [23], and (c) Mo–V system [24].

Table 1. Summary of crystal structures of solid phases in the Al–Mo–V system.

Phase/Temperature range (°C)	Prototype	Pearson symbol	Space group	Phase description
(Al), < 660	Cu	cF4	$Fm\overline{3}m$	Solid solution based on fcc_A1 Al
(Mo), < 2623	W	cI2	$Im\overline{3}m$	Solid solution based on bcc_A2 Mo
(V), < 1910	W	cI2	$Im\overline{3}m$	Solid solution based on bcc_A2 V
$Al_{12}Mo$, < 712	$Al_{12}W$	cI26	$Im\overline{3}$	Solid solution based on $Al_{12}Mo$
Al_5Mo, < 845	Al_5W	hP12	$P6_3$	Solid solution based on Al_5Mo
$Al_{22}Mo_5$, < 940	$Al_{22}Mo_5$	oF216	Fdd2	Solid solution based on $Al_{22}Mo_5$
$Al_{17}Mo_4$, < 997	$Al_{17}Mo_4$	mC84	C2	Solid solution based on $Al_{17}Mo_4$
Al_4Mo, 941~1152	Al_4W	mC30	Cm	Solid solution based on Al_4Mo
Al_3Mo, 791~1222	Al_3Mo	mC32	C2/m	Solid solution based on Al_3Mo
Al_8Mo_3, < 1528	Al_8Mo_3	mC22	C2/m	Solid solution based on Al_8Mo_3
$Al_{63}Mo_{37}$, 1489~1569	–	–	–	Binary phase $Al_{63}Mo_{37}$
AlMo, 1470~1721	W	cI2	$Im\overline{3}m$	Solid solution based on bcc_A2
$AlMo_3$, < 2148	Cr_3Si	cP8	$Pm\overline{3}n$	Solid solution based on $AlMo_3$
$Al_{21}V_2$, < 688	$Al_{21}V_2$	cF176	$Fd\overline{3}m$	Solid solution based on $Al_{21}V_2$
$Al_{45}V_7$, < 719	$Al_{45}V_7$	mC104	C2/m	Solid solution based on $Al_{45}V_7$
$Al_{23}V_4$, < 734	$Al_{23}V_4$	hP54	$P6_3/mmc$	Solid solution based on $Al_{23}V_4$
Al_3V, < 1222	Al_3Ti	tI8	I4/mmm	Solid solution based on Al_3V
Al_8V_5, < 1413	Cu_5Zn_8	cI52	$I\overline{4}3m$	Solid solution based on Al_8V_5

The phase equilibria data of the Al–Mo–V system were mainly experimentally determined by Sperner [27] and Raman [28]. In 1959, six isothermal sections at 1200, 1000, 750, 715, 675 and 630 ℃ were investigated by Sperner [27]. According to these isothermal sections, no ternary compound was found in the Al–Mo–V system. The binary phases $AlMo_3$, Al_8Mo_3, Al_3Mo, Al_5Mo and $Al_{12}Mo$ in Al–Mo binary side and Al_8V_5, Al_3V, Al_6V (or $Al_{23}V_4$, $Al_{45}V_7$) and $Al_{21}V_2$ in Al–V binary side were detected in the work of Sperner [27]. The solubilities of Mo in Al_8V_5 and Al_3V and V in $AlMo_3$ and Al_8Mo_3 slightly decrease with temperature ranges from 1200 to 630 ℃. The solubilities of Mo in Al_6V, $Al_{21}V_2$, Al_3Mo, Al_5Mo and $Al_{12}Mo$ are nearly constant in temperature ranges. The average solubilities of Mo in Al_8V_5, Al_3V, Al_6V and $Al_{21}V_2$ are about 30, 25, 10 and 6.5 wt.%, respectively, and the ones of V in $AlMo_3$, Al_8Mo_3, Al_3Mo, Al_5Mo and $Al_{12}Mo$ are about 20, 11, 6, 3 and 1.5 wt.%, respectively, in temperature ranges from 1200 to 630 ℃. The solubilities of Mo in Al–V binary phases and V in Al–Mo binary phases decrease with the decreasing of temperature. Nine invariant reactions, i.e. L + (Mo, V) ↔ Al_8V_5 + $AlMo_3$ at about 1600 ℃, L + $AlMo_3$ ↔ Al_8V_5 + Al_8Mo_3 at 1450 ℃, L + Al_8V_5 ↔ Al_3V + Al_8Mo_3 at 1300 ℃, L + Al_8Mo_3 ↔ Al_3V + Al_3Mo at 1100 ℃, L + Al_3Mo ↔ Al_3V + Al_5Mo at 720 ℃, L + Al_3V ↔ Al_6V + Al_5Mo at 700 ℃, L + Al_5Mo ↔ Al_6V + $Al_{12}Mo$ at 690 ℃, L + Al_6V ↔ $Al_{21}V_2$ + $Al_{12}Mo$ at 680 ℃, and L ↔ $Al_{12}Mo$ + $Al_{21}V_2$ + (Al) at 656 ℃, were reported and a tentative reaction scheme for the Al–Mo–V system was also constructed by Sperner [27] on the basis of the isothermal sections. The experimental data measured by Sperner [27] are included in the present optimization due to the consistency of these isothermal sections.

Twenty ternary alloys were prepared and the isothermal section at 1000 ℃ was detemined by Raman [28]. According to the experimental results [28], the binary phases $AlMo_3$, Al_8Mo_3, Al_4Mo and Al_5Mo in Al–Mo binary side and Al_8V_5 and Al_3V in Al–V binary side were detected. A ternary compound $Al_{14}Mo_5V$ closing to the binary compound Al_8Mo_3 was reported by Raman [28]. Later, Virkar and Raman [29] carried out the crystallographic investigations showing that the $Al_{14}Mo_5V$ phase has a similer structure with the Al_8Mo_3 phase and believed that the so-called ternary phase $Al_{14}Mo_5V$ is the solid solution of the alloying element V in Al_8Mo_3. Hence, the $Al_{14}Mo_5V$ phase is not included in the present optimization. In addition, the phase relations of the isothermal section at 1000 ℃ reported by Raman [28] are inconsistent with the ones from Sperner [27]. Hence, the experimental phase diagram data reported by Raman [28] is not used in the thermodynamic optimization but only used for comparison.

3. Thermodynamic model

The phases in the Al–Mo–V system to be optimized in this work are as follows: solution phases, liquid, bcc (Mo, V) and fcc (Al); binary phases extending into the ternary system, $Al_{12}Mo$, Al_5Mo, $Al_{22}Mo_5$, $Al_{17}Mo_4$, Al_4Mo, Al_3Mo, Al_8Mo_3, $AlMo_3$, $Al_{21}V_2$, $Al_{45}V_7$, $Al_{23}V_4$, Al_3V and Al_8V_5. Different models were employed to describe the above mentioned phases.

3.1 Solution phases

The solution phases, i.e. liquid, bcc (Mo, V) and fcc (Al) are described by the substitutional solution model. The molar Gibbs energy of solution phase ϕ (ϕ = liquid, bcc or fcc) is expressed by the Redlich-Kister-Muggianu polynomial [30]:

$$
\begin{aligned}
^\circ G_m^\phi = {} & x_{Al} \cdot {}^\circ G_{Al}^\phi + x_{Mo} \cdot {}^\circ G_{Mo}^\phi + x_V \cdot {}^\circ G_V^\phi \\
& + R \cdot T \cdot (x_{Al} \cdot \ln x_{Al} + x_{Mo} \cdot \ln x_{Mo} + x_V \cdot \ln x_V) \\
& + x_{Al} \cdot x_{Mo} \cdot L_{Al,Mo}^\phi + x_{Al} \cdot x_V \cdot L_{Al,V}^\phi \\
& + x_{Mo} \cdot x_V \cdot L_{Mo,V}^\phi + x_{Al} \cdot x_{Mo} \cdot x_V \\
& \cdot (x_{Al} \cdot {}^0 L_{Al,Mo,V}^\phi + x_{Mo} \cdot {}^1 L_{Al,Mo,V}^\phi + x_V \cdot {}^2 L_{Al,Mo,V}^\phi)
\end{aligned}
\tag{1}
$$

where R is the gas constant, x_{Al}, x_{Mo} and x_V are the molar fractions of the elements Al, Mo and V, respectively. The standard element reference (SER) state [21], i.e. the stable structure of the element at 25 °C and 1 bar, is used as the reference state of Gibbs energy. The parameters $L_{i,j}^\phi (i, j = Al,Mo,V)$ are the interaction parameters from binary systems. The ternary interaction parameters ${}^0 L_{Al,Mo,V}^\phi$, ${}^1 L_{Al,Mo,V}^\phi$ and ${}^2 L_{Al,Mo,V}^\phi$ are linearly temperature-dependent, which can be expressed as $L_{Al,Mo,V}^\phi = A + B \cdot T$. The coefficients A and B will be optimized from experimental data in the present work.

3.2 Binary phases

According to the experimental data from Sperner [27] and Raman [28], the binary phases $Al_{12}Mo$, Al_5Mo, Al_3Mo, Al_8Mo_3 and $AlMo_3$ in the Al–Mo system and $Al_{21}V_2$, Al_6V (or $Al_{23}V_4$, $Al_{45}V_7$), Al_3V and Al_8V_5 in the Al–V system exhibit some solubilities for V and Mo, respectively. Sublattice models [31,32] are used to describe these binary phases and listed in Table 2. In view of the experimental results [27, 28], it is assumed that Mo and V substitute each other in the sublattice models. In accordance with the formula for sublattice model, the Gibbs energy of $Al_{12}Mo$, modeled as $Al_{12}(Mo, V)_1$, taking as an example can be expressed as:

$$
\begin{aligned}
^\circ G^{Al_{12}Mo} = {} & y_{Mo}'' \cdot {}^\circ G_{Al:Mo}^{Al_{12}Mo} + y_V'' \cdot {}^\circ G_{Al:V}^{Al_{12}Mo} \\
& + R \cdot T \cdot (y_{Mo}'' \cdot \ln y_{Mo}'' + y_V'' \cdot \ln y_V'') + y_{Mo}'' \\
& \cdot y_V'' \cdot \left[{}^0 L_{Al:Mo,V}^{Al_{12}Mo} + {}^1 L_{Al:Mo,V}^{Al_{12}Mo} \left(y_{Mo}'' - y_V'' \right)^1 + ... \right]
\end{aligned}
\tag{2}
$$

where y''_{Mo} and y''_V are the site fractions of Mo and V in the second sublattice. The parameters $^{o}G^{Al_{12}Mo}_{Al:Mo}$ and $^{o}G^{Al_{12}Mo}_{Al:V}$ correspond to the Gibbs energies of the end-members $Al_{12}Mo$ and $Al_{12}V$, respectively. The interaction parameters $^{0}L^{Al_{12}Mo}_{Al:Mo,V}$ and $^{1}L^{Al_{12}Mo}_{Al:Mo,V}$ are also linearly temperature-dependent, which can be expressed as $L^{Al_{12}Mo}_{Al:Mo,V} = a + b \cdot T$, and the coefficients a and b will be optimized in the present work.

It is noted that the $AlMo_3$ and Al_8V_5 phase are modeled as $(Al, \mathbf{Mo}, V)_{0.75}(\mathbf{Al}, Mo, V)_{0.25}$ and $(\mathbf{Al}, V)_2(Al, Mo, \mathbf{V})_3(Mo, \mathbf{V})_2(\mathbf{Al})_6$, respectively. The boldfaces mean the normal atoms (i.e. major species) in the sublattices. The $Al_{22}Mo_5$, $Al_{17}Mo_4$ and Al_4Mo phases were not determined by Sperner [27]. In view of the solubilities of V in other bianry phases in the Al–Mo system, these phases were described as $(\mathbf{Al})_{22}(\mathbf{Mo}, V)_5$, $(\mathbf{Al})_{17}(\mathbf{Mo}, V)_4$, and $(\mathbf{Al})_4(\mathbf{Mo}, V)_1$, respectively, in the present work. Analogous expressions like Eq. (2) are applied to describe the Gibbs energies of the $AlMo_3$, Al_8V_5, $Al_{22}Mo_5$, $Al_{17}Mo_4$, and Al_4Mo phases.

4. Results and discussions

The thermodynamic parameters are evaluated by the optimization module PARROT [33] in the program Thermo-Calc software, which works by minimizing the square sum of the differences between the measured and calculated values. The step-by-step optimization procedure described by Du et al. [34] is utilized in the present assessment.

The optimization begins with the isothermal section at 1200 °C. According to the solubilities of V in the Al_8Mo_3 and $AlMo_3$ phases and Mo in the Al_3V and Al_8V_5 phases and the phase relations at 1200 °C determined by Sperner [27], the interaction parameters a for the Al_8Mo_3, $AlMo_3$, Al_3V and Al_8V_5 phases in Eq.(2) are optimized. Then, the isothermal sections at 1000, 750, 715, 675 and 630 °C are considered one by one in the optimization. Next, the temperatures of invariant reactions reported by Sperner [27] are evaluated. The ternary interaction parameters A for the liquid and bcc_A2 phases in Eq.(1) are obtained by fitting the experimental data of invariant reactions. Finally, all the parameters are optimized simultaneously. The thermodynamic parameters obtained in the present work are listed in Table 2.

Table 2. *Summary of the thermodynamic parameters for the Al–Mo–V system[a]*

Phase/Model	Thermodynamic parameters	Reference
Liquid: Model (Al, Mo, V)$_1$	$^{0}L^{Liquid}_{Al,Mo} = -102047.6 + 37.780 \cdot T$	[22]
	$^{1}L^{Liquid}_{Al,Mo} = 13754.5 - 1.889 \cdot T$	[22]
	$^{2}L^{Liquid}_{Al,Mo} = -37326.3 + 10.402 \cdot T$	[22]
	$^{0}L^{Liquid}_{Al,V} = -122625.8 + 17.400 \cdot T$	[23]
	$^{1}L^{Liquid}_{Al,V} = 51463.0 - 0.850 \cdot T$	[23]
	$^{0}L^{Liquid}_{Mo,V} = -1613.0 - 0.187 \cdot T$	[24]
	$^{0}L^{Liquid}_{Mo,V} = -158.0 - 0.104 \cdot T$	[24]
	$^{0}L^{Liquid}_{Al,Mo,V} = -112576.6$	This work
fcc_A1: Model (Al, Mo, V)$_1$Va$_1$	$^{0}L^{fcc\_A1}_{Al,Mo:Va} = -146174.5 + 75.699 \cdot T$	[7]
	$^{0}L^{fcc\_A1}_{Al,V:Va} = -95812.0 + 28.3 \cdot T$	[23]
bcc_A2: Model (Al, Mo, V)$_1$Va$_3$	$^{0}L^{bcc\_A2}_{Al,Mo:Va} = -73113.3 + 22.770 \cdot T$	[7]
	$^{1}L^{bcc\_A2}_{Al,Mo:Va} = -16584.5$	[7]
	$^{2}L^{bcc\_A2}_{Al,Mo:Va} = -18877.2$	[7]
	$^{0}L^{bcc\_A2}_{Al,V:Va} = -136730.0 + 14.400 \cdot T$	[23]
	$^{1}L^{bcc\_A2}_{Al,V:Va} = 131633.0 - 43.000 \cdot T$	[23]
	$^{0}L^{bcc\_A2}_{Mo,V:Va} = -4011.7 + 1.455 \cdot T$	[24]
	$^{1}L^{bcc\_A2}_{Mo,V:Va} = 187.1 + 0.208 \cdot T$	[24]
	$^{0}L^{bcc\_A2}_{Al,\mathbf{Mo},V:Va} = +6573.8$	This work

Table 2. continued on next page

Table 2. continued from previous page

Al$_{12}$Mo: Model (Al)$_{12}$(Mo, V)$_1$	$^oG_{Al:Mo}^{Al_{12}Mo} = -147884.5 + 33.000 \cdot T + 12 \cdot {}^oG_{Al}^{fcc} + {}^oG_{Mo}^{bcc}$	[22]
	$^oG_{Al:V}^{Al_{12}Mo} = -81391.5 + 12 \cdot {}^oG_{Al}^{fcc} + {}^oG_{V}^{bcc}$	This work
Al$_5$Mo: Model (Al)$_5$(Mo, V)$_1$	$^oG_{Al:Mo}^{Al_5Mo} = -148908.1 + 38.3 \cdot T + 5 \cdot {}^oG_{Al}^{fcc} + {}^oG_{Mo}^{bcc}$	[22]
	$^oG_{Al:V}^{Al_5Mo} = -83221.8 + 5 \cdot {}^oG_{Al}^{fcc} + {}^oG_{V}^{bcc}$	This work
Al$_{22}$Mo$_5$: Model (Al)$_{22}$(Mo, V)$_5$	$^oG_{Al:Mo}^{Al_{22}Mo_5} = -745899.1 + 198.5 \cdot T + 22 \cdot {}^oG_{Al}^{fcc} + 5 \cdot {}^oG_{Mo}^{bcc}$	[22]
	$^oG_{Al:V}^{Al_{22}Mo_5} = -380000 + 22 \cdot {}^oG_{Al}^{fcc} + 5 \cdot {}^oG_{V}^{bcc}$	This work
Al$_{17}$Mo$_4$: Model (Al)$_{17}$(Mo, V)$_4$	$^oG_{Al:Mo}^{Al_{17}Mo_4} = -596728.1 + 160.4 \cdot T + 17 \cdot {}^oG_{Al}^{fcc} + 4 \cdot {}^oG_{Mo}^{bcc}$	[22]
	$^oG_{Al:V}^{Al_{17}Mo_4} = -305000 + 17 \cdot {}^oG_{Al}^{fcc} + 4 \cdot {}^oG_{V}^{bcc}$	This work
Al$_4$Mo: Model (Al)$_4$(Mo, V)$_1$	$^oG_{Al:Mo}^{Al_4Mo} = -145502.1 + 35.415 \cdot T + 4 \cdot {}^oG_{Al}^{fcc} + {}^oG_{Mo}^{bcc}$	[22]
	$^oG_{Al:V}^{Al_4Mo} = -75000 + 4 \cdot {}^oG_{Al}^{fcc} + {}^oG_{V}^{bcc}$	This work
Al$_3$Mo: Model (Al)$_3$(Mo, V)$_1$	$^oG_{Al:Mo}^{Al_3Mo} = -143801.4 + 40.933 \cdot T + 3 \cdot {}^oG_{Al}^{fcc} + {}^oG_{Mo}^{bcc}$	[22]
	$^oG_{Al:V}^{Al_3Mo} = -79031.6 + 3 \cdot {}^oG_{Al}^{fcc} + {}^oG_{V}^{bcc}$	This work
Al$_8$Mo$_3$: Model (Al)$_8$(Mo, V)$_3$	$^oG_{Al:Mo}^{Al_8Mo_3} = -432300 + 128.341 \cdot T + 8 \cdot {}^oG_{Al}^{fcc} + 3 \cdot {}^oG_{Mo}^{bcc}$	[22]
	$^oG_{Al:V}^{Al_8Mo_3} = -240072.0 + 8 \cdot {}^oG_{Al}^{fcc} + 3 \cdot {}^oG_{V}^{bcc}$	This work
Al$_{63}$Mo$_{37}$: Model (Al)$_{63}$(Mo)$_{37}$	$^oG_{Al:Mo}^{Al_{63}Mo_{37}} = -1515523.6 - 176.058 \cdot T + 63 \cdot {}^oG_{Al}^{fcc} + 37 \cdot {}^oG_{Mo}^{bcc}$	[22]
AlMo$_3$: Model (Al, Mo, V)$_{0.75}$(Al, Mo, V)$_{0.25}$	$^oG_{Al:Al}^{AlMo_3} = 10000 + {}^oG_{Al}^{fcc}$	[7]
	$^oG_{Al:Mo}^{AlMo_3} = 10000 + 0.75 \cdot {}^oG_{Al}^{fcc} + 0.25 \cdot {}^oG_{Mo}^{bcc}$	[7]
	$^oG_{Mo:Al}^{AlMo_3} = -21181.0 + 3.339 \cdot T + 0.25 \cdot {}^oG_{Al}^{fcc} + 0.75 \cdot {}^oG_{Mo}^{bcc}$	[7]
	$^oG_{Mo:Al}^{AlMo_3} = 10000 + {}^oG_{Mo}^{bcc}$	[7]
	$^oG_{Al,Mo:Al}^{AlMo_3} = 0.456 \cdot T$	[7]
	$^oG_{Mo:Al,Mo}^{AlMo_3} = -2.633 \cdot T$	[7]
	$^oG_{V:V}^{AlMo_3} = +10000 + {}^oG_{V}^{bcc}$	This work
	$^oG_{Al:V}^{AlMo_3} = +0.75 \cdot {}^oG_{Al}^{fcc} + 0.25 \cdot {}^oG_{V}^{bcc}$	This work
	$^oG_{V:Al}^{AlMo_3} = -32696.4 + 0.25 \cdot {}^oG_{Al}^{fcc} + 0.75 \cdot {}^oG_{V}^{bcc}$	This work
	$^oG_{Mo:V}^{AlMo_3} = +0.75 \cdot {}^oG_{Mo}^{bcc} + 0.25 \cdot {}^oG_{V}^{bcc}$	This work
	$^oG_{V:Mo}^{AlMo_3} = +0.25 \cdot {}^oG_{Mo}^{bcc} + 0.75 \cdot {}^oG_{V}^{bcc}$	This work
	$^oG_{Mo,V:Al}^{AlMo_3} = +11863.4$	This work
Al$_{21}$V$_2$: Model (Al)$_{21}$(Mo, V)$_2$	$^oG_{Al:V}^{Al_{21}V_2} = -191571.6 - 8.28 \cdot T + 21 \cdot {}^oG_{Al}^{fcc} + 2 \cdot {}^oG_{V}^{bcc}$	[23]
	$^oG_{Al:Mo}^{Al_{21}V_2} = -199397.7 + 21 \cdot {}^oG_{Al}^{fcc} + 2 \cdot {}^oG_{Mo}^{bcc}$	This work
Al$_{45}$V$_7$: Model (Al)$_{45}$(Mo, V)$_7$	$^oG_{Al:V}^{Al_{45}V_7} = -670493.2 - 19.240 \cdot T + 45 \cdot {}^oG_{Al}^{fcc} + 7 \cdot {}^oG_{V}^{bcc}$	[23]
	$^oG_{Al:Mo}^{Al_{45}V_7} = -701507.1 + 45 \cdot {}^oG_{Al}^{fcc} + 7 \cdot {}^oG_{Mo}^{bcc}$	This work
Al$_{23}$V$_4$: Model (Al)$_{23}$(Mo, V)$_4$	$^oG_{Al:V}^{Al_{23}V_4} = -383139.0 - 9.100 \cdot T + 23 \cdot {}^oG_{Al}^{fcc} + 4 \cdot {}^oG_{V}^{bcc}$	[23]
	$^oG_{Al:Mo}^{Al_{23}V_4} = -435847.7 + 36.765 \cdot T + 23 \cdot {}^oG_{Al}^{fcc} + 4 \cdot {}^oG_{Mo}^{bcc}$	This work

Table 2. continued on next page

Table 2. continued from previous page

|		
Al$_3$V: Model (Al)$_3$(Mo, V)$_1$	$^oG_{Al:V}^{Al_3V} = -95784.2 + 0.520 \cdot T + 3 \cdot {}^oG_{Al}^{fcc} + {}^oG_V^{bcc}$	[23]
	$^oG_{Al:Mo}^{Al_3V} = -129979.4 + 36.944 \cdot T + 3 \cdot {}^oG_{Al}^{fcc} + {}^oG_{Mo}^{bcc}$	This work
	$^oG_{Al:Mo,V}^{Al_3V} = -8089.97$	This work
Al$_8$V$_5$: Model (Al, V)$_2$(Al, Mo, V)$_3$(Mo, V)$_2$(Al)$_6$	$^oG_{Al:Al:V:Al}^{Al_8V_5} = 100000 + 11 \cdot {}^oG_{Al}^{fcc} + 2 \cdot {}^oG_V^{bcc}$	[23]
	$^oG_{V:Al:V:Al}^{Al_8V_5} = 528219.9 - 26.000 \cdot T + 9 \cdot {}^oG_{Al}^{fcc} + 4 \cdot {}^oG_V^{bcc}$	[23]
	$^oG_{Al:V:V:Al}^{Al_8V_5} = -454220.0 + 26.000 \cdot T + 8 \cdot {}^oG_{Al}^{fcc} + 5 \cdot {}^oG_V^{bcc}$	[23]
	$^oG_{V:V:V:Al}^{Al_8V_5} = -26000.0 + 6 \cdot {}^oG_{Al}^{fcc} + 7 \cdot {}^oG_V^{bcc}$	[23]
	$^oG_{Al,V:Al:V:Al}^{Al_8V_5} = -465244.0$	[23]
	$^oG_{Al,V:V:V:Al}^{Al_8V_5} = -465244.0$	[23]
	$^oG_{Al:Al,V:V:Al}^{Al_8V_5} = -299767.0$	[23]
	$^oG_{V:Al,V:V:Al}^{Al_8V_5} = -299767.0$	[23]
	$^oG_{Al:Mo:Mo:Al}^{Al_8V_5} = +8 \cdot {}^oG_{Al}^{fcc} + 5 \cdot {}^oG_{Mo}^{bcc}$	This work
	$^oG_{Al:Al:Mo:Al}^{Al_8V_5} = +11 \cdot {}^oG_{Al}^{fcc} + 2 \cdot {}^oG_{Mo}^{bcc}$	This work
	$^oG_{Al:V:Mo:Al}^{Al_8V_5} = +8 \cdot {}^oG_{Al}^{fcc} + 2 \cdot {}^oG_{Mo}^{bcc} + 3 \cdot {}^oG_V^{bcc}$	This work
	$^oG_{V:Mo:Mo:Al}^{Al_8V_5} = +6 \cdot {}^oG_{Al}^{fcc} + 5 \cdot {}^oG_{Mo}^{bcc} + 2 \cdot {}^oG_V^{bcc}$	This work
	$^oG_{V:Mo:V:Al}^{Al_8V_5} = +6 \cdot {}^oG_{Al}^{fcc} + 3 \cdot {}^oG_{Mo}^{bcc} + 4 \cdot {}^oG_V^{bcc}$	This work
	$^oG_{V:Al:Mo:Al}^{Al_8V_5} = +9 \cdot {}^oG_{Al}^{fcc} + 2 \cdot {}^oG_{Mo}^{bcc} + 2 \cdot {}^oG_V^{bcc}$	This work
	$^oG_{V:V:Mo:Al}^{Al_8V_5} = +6 \cdot {}^oG_{Al}^{fcc} + 2 \cdot {}^oG_{Mo}^{bcc} + 5 \cdot {}^oG_V^{bcc}$	This work
	$^oG_{Al:Mo:V:Al}^{Al_8V_5} = -420988.6 + 67.328 \cdot T + 8 \cdot {}^oG_{Al}^{fcc} + 3 \cdot {}^oG_{Mo}^{bcc} + 2 \cdot {}^oG_V^{bcc}$	This work
	$^oG_{Al:Mo,V:V:Al}^{Al_8V_5} = -147052.5$	This work

ᵃ All parameters are given in J/(mole-atoms); Temperature (T) in K. The Gibbs energies for the pure elements Al, Mo and V are taken from the SGTE database compiled by Dinsdale [21].

In figure 2, the calculated isothermal section at 1200 °C of the Al–Mo–V system is compared with the observed one by Sperner [27]. As can be seen from these figures, the calculated results can account for most of the experimental data [27] in view of experimental errors. It is noteworthy that there is a sharp edge on the AlMo$_3$ phase in the two-phase region AlMo$_3$ + bcc (Mo, V) at 1200 °C in Fig. 2(b). It can be interpreted by the following two reasons. On the one hand, the shape of AlMo$_3$ is determined by the thermodynamic parameters of both the AlMo$_3$ phase and other phases around AlMo$_3$, which are globally optimized based on the phase equilibria data. On the other hand, a sharp edge on the AlMo$_3$ phase in the two-phase region AlMo$_3$ + bcc (Mo, V) is expected to exist at a temperature above 1000°C. This can be deduced from the difference between the phase relations of the isothermal sections at 1200 and 1000 °C. A miscibility gap of bcc (Mo) + bcc (V) appears at 1000 °C in Fig. 3. Thus, there exists the three-phase region of AlMo$_3$ + bcc (Mo) + bcc (V). The compositions of AlMo$_3$ for the two three-phase

regions AlMo$_3$ + bcc (Mo) + bcc (V) and AlMo$_3$ + Al$_8$V$_5$ + bcc (V) at 1000 °C are not identical and the miscibility gap of bcc (Mo) + bcc (V) disappears above 1000 °C. In other words, the three-phase region of AlMo$_3$ + bcc (Mo) + bcc (V) does not exist above 1000 °C. Hence, based on the phase rule, there should be a sharp edge on the AlMo$_3$ in the two-phase region AlMo$_3$ + bcc (Mo, V) at the temperatures above 1000 °C, which will disappear at higher temperatures. The exact temperature should be measured in the future experiments, which is not the purpose of the present work.

Figure 3 shows the calculated isothermal section at 1000 °C in comparison with the experimental data reported by Sperner [27] and Raman [28]. The calculations can reproduce most of the experimental data from Sperner [27]. The Al$_4$Mo phase was not found at 1000 °C in the work of Sperner [27], which is inconsistent with the accepted Al–Mo phase diagram [22], as shown in Fig.1 (a). The calculated three-phase regions liquid + Al$_4$Mo + Al$_3$V and Al$_4$Mo + Al$_3$V + Al$_3$Mo need further experimental verifications. As
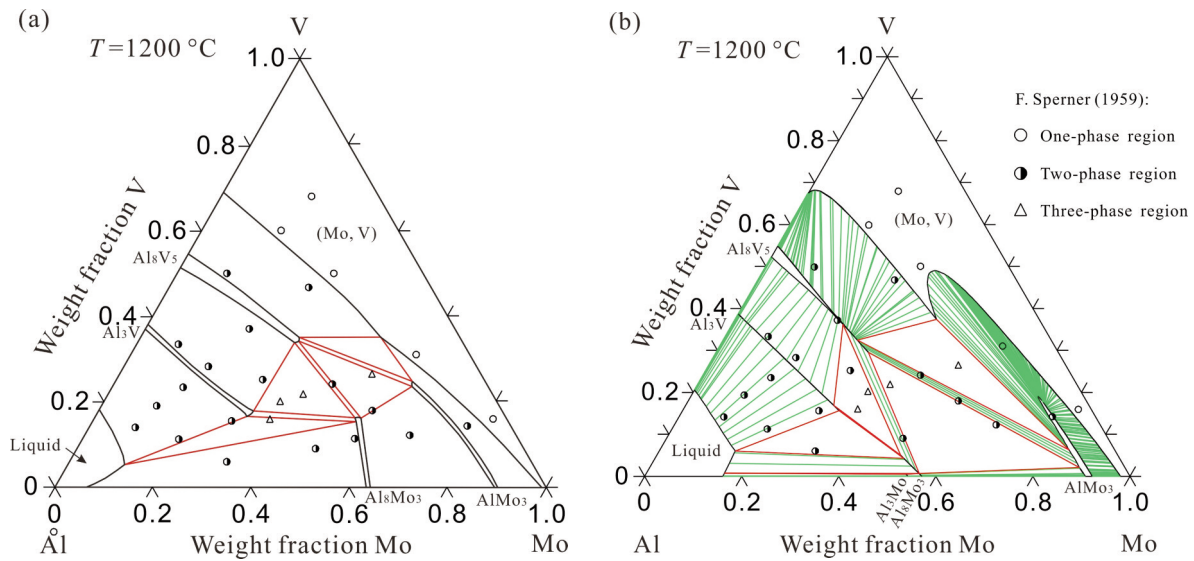
Figure 2. *Observed and calculated isothermal sections at 1200 °C of the Al–Mo–V system: (a) observed section by Sperner [27] and (b) calculated section according to the present work along with the experimental data from Sperner [27].*

mentioned above, the experimental data from Raman [28] are not used in the present optimization but only used for comparison due to the contradictions of the experimental results between Sperner [27] and Raman [28]. In addition, the present calculations show that there exists a miscibility gap of bcc (Mo) + bcc (V) closing to the Mo–V binary side below 1000 °C. The existence of the miscibility gap also needs to be confirmed by further experiments.
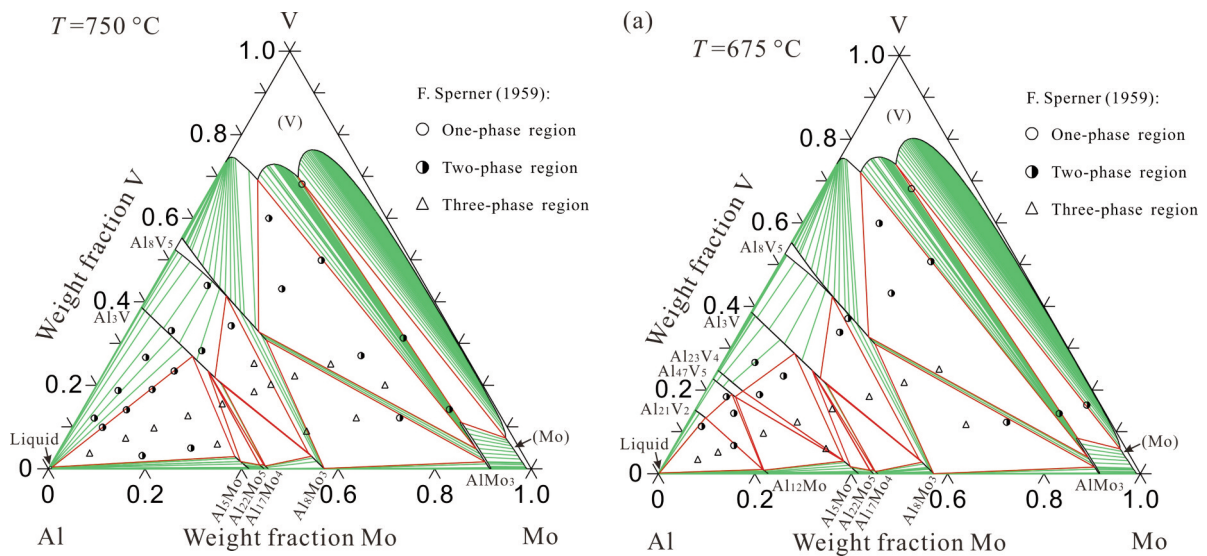
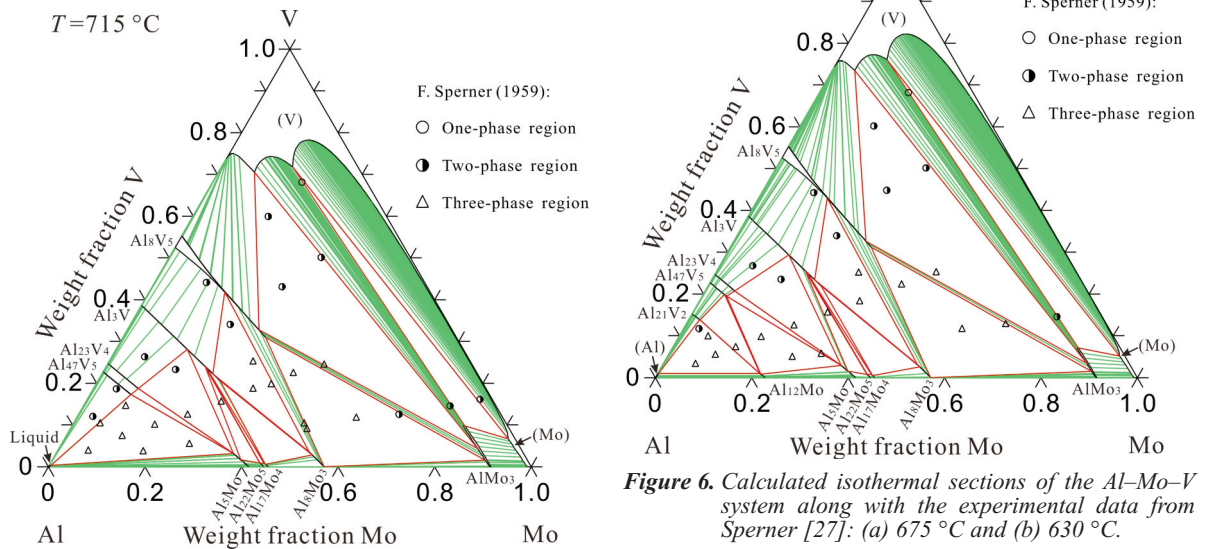In figure 4, the calculated isothermal section at 750 °C is compared with the experimental data from
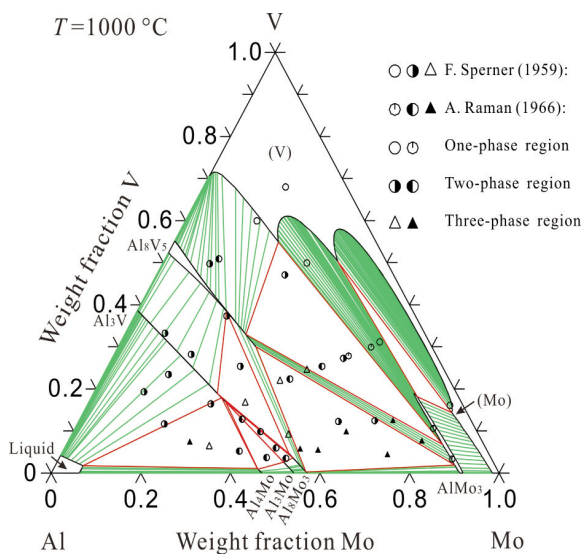
Figure 3. *Calculated isothermal section at 1000 °C of the Al–Mo–V system, compared with the experimental data from Sperner [27] and Raman [28].*

Sperner [27]. In comparison with the experimental data, some discrepancies exist in Al–Mo binary side. According to the experimental data from Sperner [27], the binary phase Al_3Mo was determined but the Al_5Mo, $Al_{22}Mo_5$ and $Al_{17}Mo_4$ phases not at 750 °C. The experimental results are inconsistent with the accepted Al–Mo binary phase diagram in Fig.1 (a). The Al_5Mo, $Al_{22}Mo_5$ and $Al_{17}Mo_4$ phases are stable at 750 °C but Al_3Mo not. Thus, the phase relations liquid + Al_3Mo + Al_3V and Al_3Mo + Al_8Mo_3 + Al_3V reported by Sperner [27] are modified to be liquid + Al_5Mo + Al_3V, Al_5Mo + $Al_{22}Mo_5$ + Al_3V, $Al_{22}Mo_5$ + $Al_{17}Mo_4$ + Al_3V, and $Al_{17}Mo_4$ + Al_8Mo_3 + Al_3V in the present work. In addition, due to the existence of the miscibility gap of bcc (Mo) + bcc (V), the calculated composition (i.e. 10 wt.% Mo and 70 wt.% V) of the bcc (V) phase for the three-phase region $AlMo_3$ + Al_8V_5 + bcc (V) deviates from the experimental one of 44.7 wt.% Mo and 47.6 wt.% V by Sperner [27]. It leads to three data points of half-black circle in V-rich corner in two-phase region of Al_8V_5 + bcc (V) measured by Sperner [27] to be in three-phase region of Al_8V_5 + bcc (V) + $AlMo_3$ in the present work.

Figure 5 presents the calculated isothermal section at 715 °C along with the experimental data from Sperner [27]. Just as the isothermal section at 750 °C, there are some discrepancies between the calculated and experimental isothermal section at 715 °C. Besides the issues of the $Al_{22}Mo_5$ and $Al_{17}Mo_4$ phases and the miscibility gap of bcc (Mo) + bcc (V) mentioned above, the calculated phase relations in Al-rich corner along the Al–V binary side are inconsistent with the experimental data reported by Sperner [27]. The Al_6V binary phase was determined
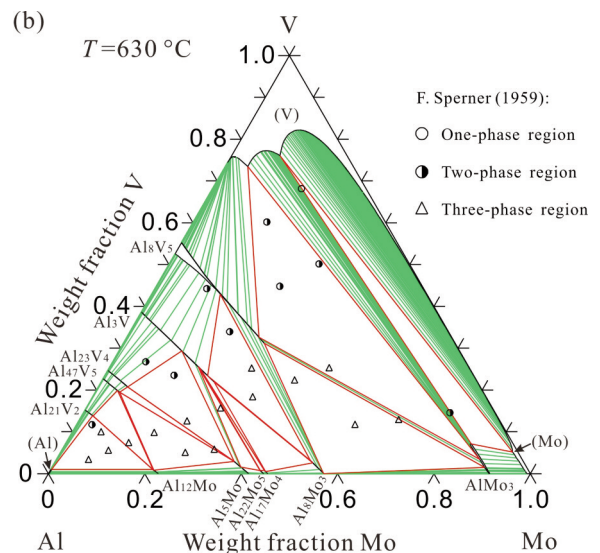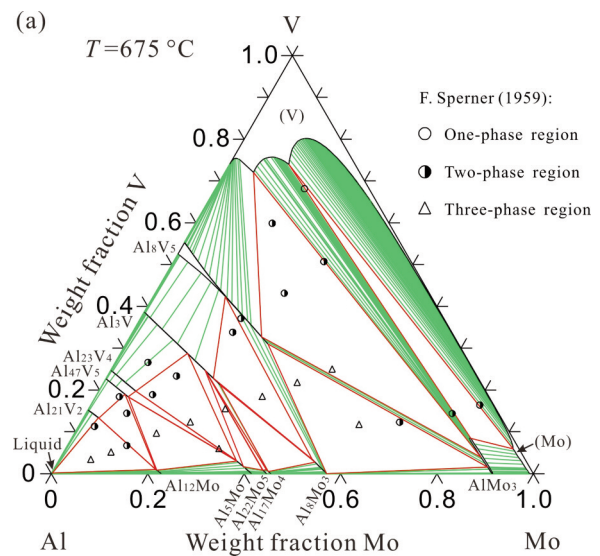
Figure 4. *Calculated isothermal section at 750 ºC of the Al–Mo–V system, compared with the experimental data from Sperner [27].*

Figure 5. *Calculated isothermal section at 715 ºC of the Al–Mo–V system, compared with the experimental data from Sperner [27].*

Figure 6. *Calculated isothermal sections of the Al–Mo–V system along with the experimental data from Sperner [27]: (a) 675 °C and (b) 630 °C.*

in the isothermal section at 715 ºC by Sperner [27]. Actually, the Al_6V phase is replaced by the $Al_{23}V_4$ and $Al_{45}V_7$ phases in the accepted Al–V phase diagram [23] in Fig.1 (b). Hence, the phase relations liquid + Al_6V + Al_3V and liquid + Al_5Mo + Al_3V reported by Sperner [27] are modified to be liquid + Al_5Mo + $Al_{45}V_7$, Al_5Mo + $Al_{45}V_7$ + $Al_{23}V_4$, and Al_5Mo + $Al_{23}V_4$ + Al_3V in the present work.

The calculated isothermal sections at 675 and 630 ºC of the Al–Mo–V system in comparison with the experimental data from Sperner [27] are shown in Fig. 6 (a) and (b), respectively. As can be seen from this figure, most of the reliable experimental data reported

by Sperner [27] can be reproduced well by the present modeling except for the phase relations of the $Al_{22}Mo_5$, $Al_{17}Mo_4$, $Al_{23}V_4$ and $Al_{45}V_7$ phases and the miscibility gap of bcc (Mo) + bcc (V) mentioned above. The calculated phase relations at 675 ºC are the same with the ones at 630 ºC except for the liquid (Al) at 675 ºC and fcc (Al) at 630 ºC.

Based on the above discussion, almost all the reliable experimental phase diagram data are satisfactorily accounted for by the present modeling except for the phase relations of the Al_4Mo, $Al_{22}Mo_5$, $Al_{17}Mo_4$, $Al_{23}V_4$ and $Al_{45}V_7$ phases and the miscibility gap of bcc (Mo) + bcc (V). According to the experimental data from Sperner [27], the Al_4Mo, $Al_{22}Mo_5$ and $Al_{17}Mo_4$ phases were not determined and

the $Al_{23}V_4$ and $Al_{45}V_7$ phases were replaced by the Al_6V phase. The results of Sperner [27] do not agree with the accepted Al–Mo and Al–V binary phase diagrams, as shown in Fig.1 (a) and (b), respectively. Thus, the calculated and experimental isothermal sections show some differences. Further experiments are needed to confirm the accuracy of the calculated phase relations related to these binary phases Al_4Mo, $Al_{22}Mo_5$, $Al_{17}Mo_4$, $Al_{23}V_4$ and $Al_{45}V_7$. Furthermore, the calculated isothermal sections show there is a miscibility gap of bcc (Mo) + bcc (V) closing to the Mo–V binary side below 1000 ºC. Further experiments are also necessary to verify the existence of the miscibility gap.

On the basis of the optimization of the experimental data reported by Sperner [27], the liquidus projection with isotherm of the Al–Mo–V system is also calculated in the present work, as shown in Fig. 7 (a). Fig.7 (b) is the enlargement of the triangle in Fig. 7 (a) and Fig.7 (c) is the enlargement of the circle in Fig. 7 (b). A comparison between the calculated and literature reported invariant reactions is listed in Table 3. Figure 8 presents the partial reaction scheme for the Al–Mo–V system. A general agreement is obtained between the calculations and the experiments [27]. For the type of the invariant reactions, the calculated invariant reactions are L $\leftrightarrow$ Al_8V_5 + $AlMo_3$ + (Mo, V), L + Al_8V_5 + Al_8Mo_3 $\leftrightarrow$

Table 3. Calculated temperatures for the invariant reactions on the liquidus surface in the Al–Mo–V system compared with the experimental values.

| Type	Invariant Reaction	Temperature/ºC	Source
U_1	L + $Al_{63}Mo_{37}$ $\leftrightarrow$ Al_8Mo_3 + AlMo	1502	Calculated (This work)
U_2	L + AlMo $\leftrightarrow$ Al_8Mo_3 + $AlMo_3$	1409	Calculated (This work)
U_3	L + Al_8Mo_3 $\leftrightarrow$ Al_8V_5 + $AlMo_3$	1334	Calculated (This work)
E_1	L + (Mo, V) $\leftrightarrow$ Al_8V_5 + $AlMo_3$	~ 1600	Measured [27]
	L $\leftrightarrow$ Al_8V_5 + $AlMo_3$ + (Mo, V)	1329	Calculated (This work)
P_1	L + Al_8V_5 $\leftrightarrow$ Al_3V + Al_8Mo_3	~ 1300	Measured [27]
	L + Al_8V_5 + Al_8Mo_3 $\leftrightarrow$ Al_3V	1292	Calculated (This work)
U_4	L + Al_8Mo_3 $\leftrightarrow$ Al_3V + Al_3Mo	~ 1100	Measured [27]
		1102	Calculated (This work)
U_5	L + Al_3Mo $\leftrightarrow$ Al_3V + Al_4Mo	1069	Calculated (This work)
U_6	L + Al_4Mo $\leftrightarrow$ Al_3V + $Al_{17}Mo_4$	995	Calculated (This work)
U_7	L + $Al_{17}Mo_4$ $\leftrightarrow$ Al_3V + $Al_{22}Mo_5$	910	Calculated (This work)
P_2	L + Al_3V + $Al_{22}Mo_5$ $\leftrightarrow$ Al_5Mo	904	Calculated (This work)
U_8	L + Al_3V $\leftrightarrow$ Al_6V + Al_5Mo	700	Measured [27]
	L + Al_3V $\leftrightarrow$ $Al_{23}V_4$ + Al_5Mo	717	Calculated (This work)
U_9	L + $Al_{23}V_4$ $\leftrightarrow$ $Al_{45}V_7$ + Al_5Mo	715	Calculated (This work)
U_{10}	L + Al_5Mo $\leftrightarrow$ Al_6V + $Al_{12}Mo$	690	Measured [27]
	L + Al_5Mo $\leftrightarrow$ $Al_{45}V_7$ + $Al_{12}Mo$	703	Calculated (This work)
U_{11}	L + Al_6V $\leftrightarrow$ $Al_{21}V_2$ + $Al_{12}Mo$	680	Measured [27]
	L + $Al_{45}V_7$ $\leftrightarrow$ $Al_{21}V_2$ + $Al_{12}Mo$	683	Calculated (This work)
U_{12}	L $\leftrightarrow$ $Al_{12}Mo$ + $Al_{21}V_2$ + (Al)	656	Measured [27]
	L + $Al_{21}V_2$ $\leftrightarrow$ $Al_{12}Mo$ + (Al)	664	Calculated (This work)
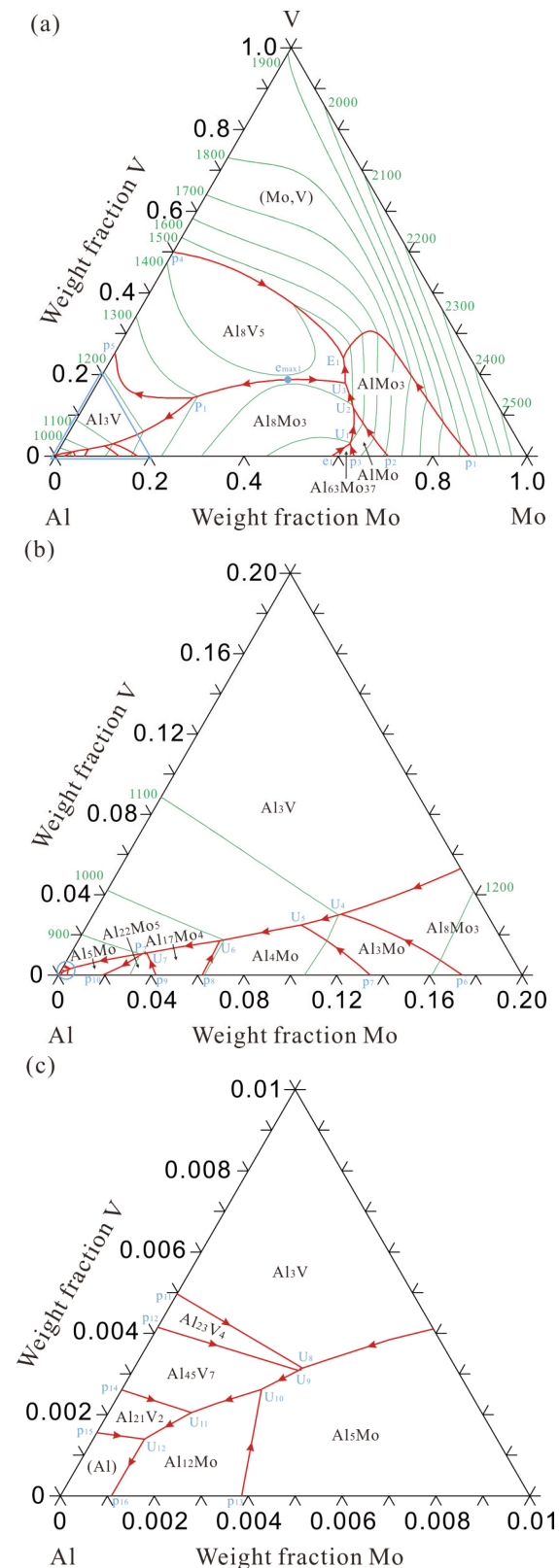
Figure 7. Calculated liquidus surface projection in the Al–Mo–V system: (a) the whole composition, (b) enlarged triangle in (a), and (c) enlarged circle in (b).

Al_3V, and $L + Al_{21}V_2 \leftrightarrow Al_{12}Mo + (Al)$, whereas the reported ones [27] are $L + (Mo, V) \leftrightarrow Al_8V_5 + AlMo_3$, $L + Al_8V_5 \leftrightarrow Al_3V + Al_8Mo_3$, and $L \leftrightarrow Al_{12}Mo + Al_{21}V_2 + (Al)$, respectively. For the temperatures of the invariant reactions, the calculated results are in good agreement with the reported ones within the estimated experimental errors except for the invariant reaction $L \leftrightarrow Al_8V_5 + AlMo_3 + (Mo, V)$. The difference between the calculated and the reported temperature of the invariant reaction $L \leftrightarrow Al_8V_5 + AlMo_3 + (Mo, V)$ is about 271 °C. Further experiments are needed to verify the type and temperature of the invariant reactions because these invariant reactions reported by Sperner [27] are tentative and obtained by considering the determined isothermal sections. In addition, Sperner [27] also reported two ternary invariant reactions $L + AlMo_3 \leftrightarrow Al_8V_5 + Al_8Mo_3$ and $L + Al_3Mo \leftrightarrow Al_3V + Al_5Mo$ derived from binary invariant reactions $L \leftrightarrow AlMo_3 + Al_8Mo_3$ at 1760 °C and $L + Al_3Mo \leftrightarrow Al_5Mo$ at 735 °C in the Al–Mo system. According to the accepted Al–Mo phase diagram in Fig.1 (a), these binary invariant reactions do not exist. Thus, the ternary invariant reactions $L + AlMo_3 \leftrightarrow Al_8V_5 + Al_8Mo_3$ and $L + Al_3Mo \leftrightarrow Al_3V + Al_5Mo$ reported by Sperner [27] are obviously wrong.

The present work demonstrates that the CALPHAD approach is a powerful tool to evaluate a ternary system with limited experimental data. It is possible to describe the complicated phase equiliria of a system over the entire composition in a wide temperature range based on limited reliable experimental information. The CALPHAD approach is highly recommended in the present work. It is expected that this approach can be applied to other systems in order to develop reliable thermodynamic descriptions of multi-component alloys.

5. Conclusions

The experimental phase equilibria data for the Al–Mo–V system available in the literature are critically evaluated. Based on these experimental data, the Al–Mo–V system is evaluated by means of the CALPHAD approach. A set of self-consistent thermodynamic parameters of the Al–Mo–V system is obtained. Some representative isothermal sections and liquidus surface projection are calculated. The calculated results are in good agreement with the most of the experimental data. In spite of the fact that the CALPHAD method is a powerful tool to optimize a system based on the limited experimental data, no updated descriptions of the binary phases in the Al-Mo and Al-V systems in the work of Sperner [27] and
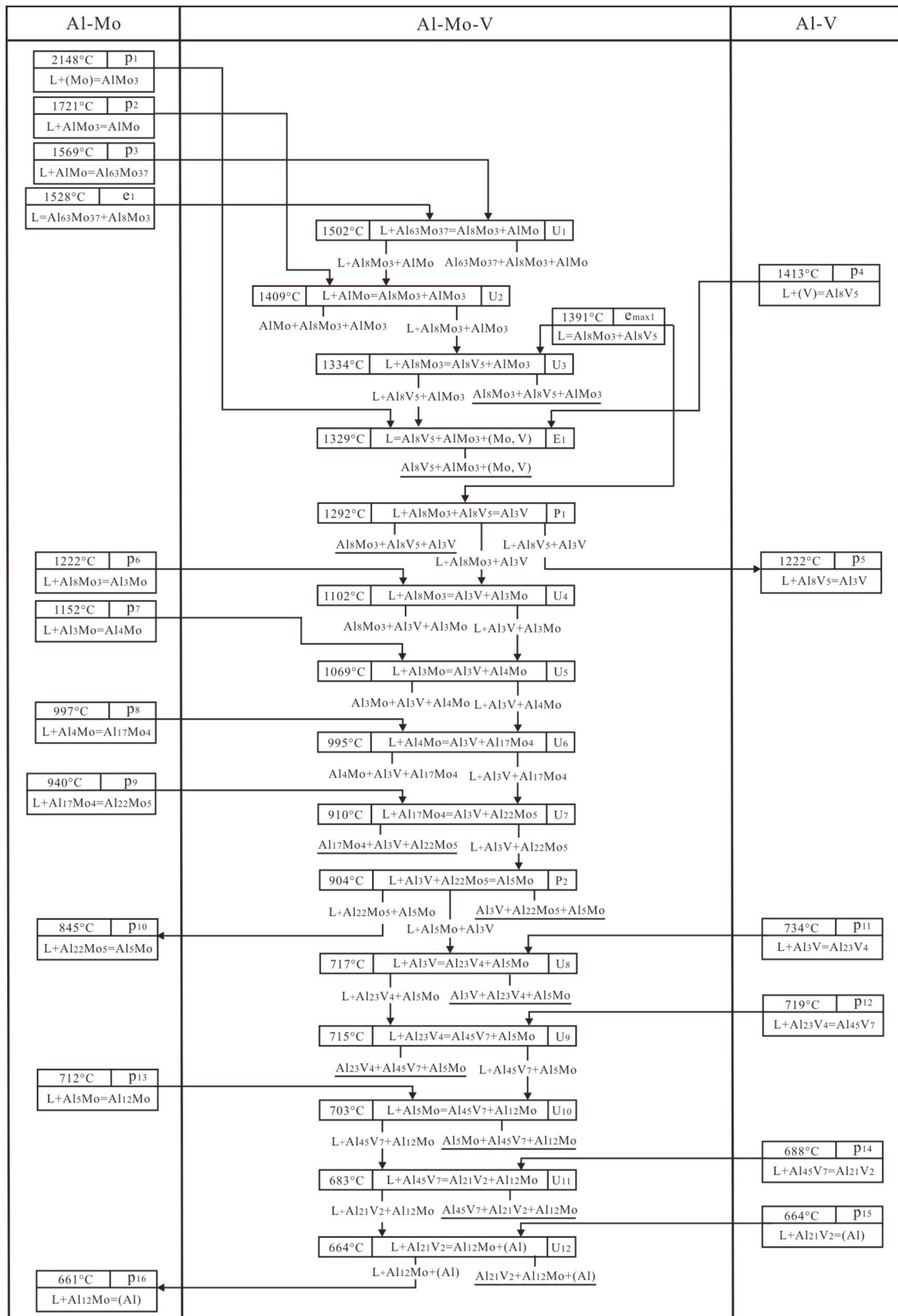
Al-Mo	Al-Mo-V	Al-V

Al-Mo column:

2148°C   p₁
L+(Mo)=AlMo₃

1721°C   p₂
L+AlMo₃=AlMo

1569°C   p₃
L+AlMo=Al₆₃Mo₃₇

1528°C   e₁
L=Al₆₃Mo₃₇+Al₈Mo₃

1222°C   p₆
L+Al₈Mo₃=Al₃Mo

1152°C   p₇
L+Al₃Mo=Al₄Mo

997°C   p₈
L+Al₄Mo=Al₁₇Mo₄

940°C   p₉
L+Al₁₇Mo₄=Al₂₂Mo₅

845°C   p₁₀
L+Al₂₂Mo₅=Al₅Mo

712°C   p₁₃
L+Al₅Mo=Al₁₂Mo

661°C   p₁₆
L+Al₁₂Mo=(Al)

Al-Mo-V column:

1502°C   L+Al₆₃Mo₃₇=Al₈Mo₃+AlMo   U₁
L+Al₈Mo₃+AlMo   Al₆₃Mo₃₇+Al₈Mo₃+AlMo

1409°C   L+AlMo=Al₈Mo₃+Al₃Mo₃   U₂
AlMo+Al₈Mo₃+Al₃Mo₃   L+Al₈Mo₃+Al₃Mo₃

1334°C   L+Al₈Mo₃=Al₈V₅+Al₃Mo₃   U₃
L+Al₈V₅+Al₃Mo₃   Al₈Mo₃+Al₈V₅+Al₃Mo₃

1329°C   L=Al₈V₅+AlMo₃+(Mo, V)   E₁
Al₈V₅+AlMo₃+(Mo, V)

1292°C   L+Al₈Mo₃+Al₈V₅=Al₃V   P₁
Al₈Mo₃+Al₈V₅+Al₃V   L+Al₈V₅+Al₃V
L+Al₈Mo₃+Al₃V

1102°C   L+Al₈Mo₃=Al₃V+Al₃Mo   U₄
Al₈Mo₃+Al₃V+Al₃Mo   L+Al₃V+Al₃Mo

1069°C   L+Al₃Mo=Al₃V+Al₄Mo   U₅
Al₃Mo+Al₃V+Al₄Mo   L+Al₃V+Al₄Mo

995°C   L+Al₄Mo=Al₃V+Al₁₇Mo₄   U₆
Al₄Mo+Al₃V+Al₁₇Mo₄   L+Al₃V+Al₁₇Mo₄

910°C   L+Al₁₇Mo₄=Al₃V+Al₂₂Mo₅   U₇
Al₁₇Mo₄+Al₃V+Al₂₂Mo₅   L+Al₃V+Al₂₂Mo₅

904°C   L+Al₃V+Al₂₂Mo₅=Al₅Mo   P₂
L+Al₂₂Mo₅+Al₅Mo   Al₃V+Al₂₂Mo₅+Al₅Mo
L+Al₅Mo+Al₃V

717°C   L+Al₃V=Al₂₃V₄+Al₅Mo   U₈
L+Al₂₃V₄+Al₅Mo   Al₃V+Al₂₃V₄+Al₅Mo

715°C   L+Al₂₃V₄=Al₄₅V₇+Al₅Mo   U₉
Al₂₃V₄+Al₄₅V₇+Al₅Mo   L+Al₄₅V₇+Al₅Mo

703°C   L+Al₅Mo=Al₄₅V₇+Al₁₂Mo   U₁₀
L+Al₄₅V₇+Al₁₂Mo   Al₅Mo+Al₄₅V₇+Al₁₂Mo

683°C   L+Al₄₅V₇=Al₂₁V₂+Al₁₂Mo   U₁₁
L+Al₂₁V₂+Al₁₂Mo   Al₄₅V₇+Al₂₁V₂+Al₁₂Mo

664°C   L+Al₂₁V₂=Al₁₂Mo+(Al)   U₁₂
L+Al₁₂Mo+(Al)   Al₂₁V₂+Al₁₂Mo+(Al)

Al-V column:

1413°C   p₄
L+(V)=Al₈V₅

1391°C   e_max1
L=Al₈Mo₃+Al₈V₅

1222°C   p₅
L+Al₈V₅=Al₃V

734°C   p₁₁
L+Al₃V=Al₂₃V₄

719°C   p₁₂
L+Al₂₃V₄=Al₄₅V₇

688°C   p₁₄
L+Al₄₅V₇=Al₂₁V₂

664°C   p₁₅
L+Al₂₁V₂=(Al)

Figure 8. *Partial reaction scheme of the Al–Mo–V system according to the present work.*

the absence of the thermodynamic experimental data (such as mixing enthalpy, activity, etc.) in the Al–Mo–V system may lead to the obtained thermodynamic parameters in the present work failing to account for some new phase equilibria data and thermodynamic data. Therefore, further experiments are necessary to verify the phase relations related to the binary phases Al_4Mo, $Al_{22}Mo_5$, $Al_{17}Mo_4$, $Al_{23}V_4$ and $Al_{45}V_7$ and the existence of the miscibility gap of bcc (Mo) + bcc (V).

Reference

[1] M. Eumann, M. Palm, G. Sauthoff, Intermetallics, 12 (2004) 625-633.

[2] H. Bei, E.P. George, Acta Mater., 53 (2005) 69-77.

[3] M. Dudová, K. Kuchařová, T. Barták, H. Bei, E.P. George, C. Somsen, A. Dlouhý, Scr. Mater., 65 (2011) 699-702.

[4] S. Milenkovic, A.A. Coelho, R. Caram, J. Cryst. Growth, 211 (2000) 485-490.

[5] G. Lutjering, J.C. Williams, Titanium, Springer, New York, 2007.

[6] I.S. Jung, H.S. Jang, M.H. Oh, J.H. Lee, D.M. Wee, Mater. Sci. Eng. A, 329-331 (2002) 13-18.

[7] D.M. Cupid, O. Fabrichnaya, F. Ebrahimi, H.J. Seifert, Intermetallics, 18 (2010) 1185-1196.

[8] X.G. Lu, N. Gui, A.T. Qiu, G.X. Wu, C.H. Li, Metall. Mater. Trans. A, 45A (2014) 4155-4164.

[9] J. Wang, H.H. Xu, S.L. Shang, L.J. Zhang, Y. Du, W.Q. Zhang, S.H. Liu, P.S. Wang, Z.-K. Liu, Calphad, 35 (2011) 191-203.

[10] B. Hu, W.-W. Zhang, Y.B. Peng, Y. Du, S.H. Liu, Y.L. Zhang, Thermochim. Acta, 561 (2013) 77-90.

[11] D. Hao, B. Hu, K. Zhang, L.J. Zhang, Y. Du, J. Mater. Sci., 49 (2014) 1157-1169.

[12] B. Hu, Y. Du, J.C. Schuster, W.H. Sun, S.H. Liu, C.Y. Tang, Thermochim. Acta, 578 (2014) 35-42.

[13] B. Hu, S. Qin, Y. Du, Z.Y. Li, Q.P. Wang, J. Phase Equilib. Diff., 36 (2015) 333-349.

[14] B. Hu, Y. Du, J.-J. Yuan, Z.-F. Liu, Q.-P. Wang, J. Min. Metall. Sect. B-Metall., 51(2) B (2015) 125–132.

[15] J. Zhao, J. Zhou, S. Liu, Y. Du, S. Tang, Y. Yang, J. Min. Metall. Sect. B-Metall., 52(1) B (2016) 99-112.

[16] B. Hu, J. Wang, C. Wang, Y. Du, J.B. Zhu, Calphad, 55 (2016) 103-112.

[17] B. Hu, X.M. Yuan, Y. Du, J. Wang, Z.-K. Liu, J. Alloys Compd., 693 (2017) 344-356.

[18] http://www.thermocalc.com.

[19] Z.-K. Liu, Y. Wang, Computational thermodynamics of materials, Cambridge University Press, Cambridge, 2016.

[20] H. Lukas, S.G. Fries, B. Sundman, Computational thermodynamics: the CALPHAD method, Cambridge University Press, Cambridge, 2007.

[21] A.T. Dinsdale, Calphad, 15 (1991) 317-425.

[22] J. Peng, P. Franke, D. Manara, T. Watkins, R.J.M. Konings, H.J. Seifert, J. Alloys Compd., 674 (2016) 305-314.

[23] W.P. Gong, Y. Du, B.Y. Huang, R. Schmid-Fetzer, C.F. Zhang, H.H. Xu, Z. Metallkd., 95 (2004) 978-986.

[24] F. Zheng, B.B. Argent, J.F. Smith, J. Phase Equilib., 20 (1999) 370-372.

[25] J. Bratberg, K. Frisk, Calphad, 26 (2002) 459-476.

[26] B. Lindahl, X.L. Liu, Z.-K. Liu, M. Selleby, Calphad, 51 (2015) 75-88.

[27] F. Sperner, Z. Metallkd., 50 (1959) 592-596 (in German).

[28] A. Raman, Z. Metallkd., 57 (1966) 535-540 (in German).

[29] A.V. Virkar, A. Raman, Z. Metallkd., 60 (1959) 594-600.

[30] O. Redlich, A.T. Kister, Ind. Eng. Chem., 40 (1948) 345-348.

[31] M. Hillert, L.I. Staffansson, Acta Chem. Scand., 24 (1970) 3618-3626.

[32] B. Sundman, J. Ågren, J. Phys. Chem. Solids, 42 (1981) 297-301.

[33] B. Sundman, B. Jansson, J.-O. Andersson, CALPHAD, 9 (1985) 153-190.

[34] Y. Du, R. Schmid-Fetzer, H. Ohtani, Z. Metallkd., 88 (1997) 545-556.